Article:
Qin, X, Engwer, C, Desai, S et al. (2 more authors) (2017) An investigation of the interactions between an E. coli bacterial quorum sensing biosensor and chitosan-based nanocapsules. Colloids and Surfaces B: Biointerfaces, 149. pp. 358-368. ISSN 0927-7765

https://doi.org/10.1016/j.colsurfb.2016.10.031

Colloids and Surfaces B: Biointerfaces 149 (2017) 358-368

An investigation of the interactions between an E. coli bacterial quorum sensing biosensor and chitosan-based nanocapsules

Xiaofei Qin[1§], Christoph Engwer[1§], Saaketh Desai[2], Celina Vila-Sanjurjo[1],
Francisco M. Goycoolea[1*]

[1]Institute of Plant Biology and Biotechnology, University of Münster. Schlossgarten 3, D-48149 Münster, Germany. fm.goycoolea@gmail.com

[2] Department of Metallurgical and Materials Engineering, Indian Institute of Technology Roorkee, Roorkee (India)

Colloids and Surfaces B: Biointerfaces 149 (2017) 358-368
http://dx.doi.org/10.1016/j.colsurfb.2016.10.031
Available online: 17 October 2016

Highlights

- Chitosan-coated nanocapsules, but not nanoemulsions, influence the ζ-potential of E.coli
- A fixed number of nanocapsules binds and promotes aggregation of bacteria
- In silico simulations agree closely with experimental results
- Chitosan-coated nanocapsules attenuate the bacterial quorum sensing response

§ These authors contributed equally to this publication
* Author for correspondence

Colloids and Surfaces B: Biointerfaces 149 (2017) 358-368

Abstract

We examined the interaction between chitosan-based nanocapsules (NC), with average hydrodynamic diameter ~114-155 nm, polydispersity ~0.127, and ζ-potential ~+50 mV, and an E. coli bacterial quorum sensing reporter strain. Dynamic light scattering (DLS) and nanoparticle tracking analysis (NTA) allowed full characterization and assessment of the absolute concentration of NC per unit volume in suspension. By centrifugation, DLS, and NTA, we determined experimentally a "stoichiometric" ratio of ~80 NC/bacterium. By SEM it was possible to image the aggregation between NC and bacteria. Moreover, we developed a custom in silico platform to simulate the behavior of particles with diameters of 150 nm and ζ–potential of +50 mV on the bacterial surface. We computed the detailed force interactions between NC-NC and NC-bacteria and found that a maximum number of 145 particles might interact at the bacterial surface. Additionally, we found that the "stoichiometric" ratio of NC and bacteria has a strong influence on the bacterial behavior and influences the quorum sensing response, particularly due to the aggregation driven by NC.

Key words: nanocapsules, chitosan, quorum sensing, bacteria, interactions

1. Introduction

The study of the interaction between nanomaterials and bacteria is relevant in several areas and problems in the life sciences, such as development of antibacterial strategies for overcoming antibiotic resistance, and biosensors development. [1,2]. However, the indiscriminate use of nanomaterials in antibacterial control can have major environmental and toxicological consequences. Nanomaterials based on natural building blocks, such as biopolymers, lipids, or proteins, however, can offer to be a safe, environmentally friendly, and attractive alternative to metal- or other inorganic-based ones. These type of nanomaterials have also been found with the special ability to interact with bacteria by fusing with their outer membrane by different mechanisms in Gram-negative and Gram-positive bacteria [3].

In the case of nanomaterials comprising polycations (e.g., chitosan and its derivatives) that exhibit a positively-charged surface, the main driving force for their interaction with bacteria is electrostatic in nature [4–6]. Other nanomaterials bearing a positively-charged surface, such as diamond nanoparticles, bind closely to the surface of bacteria [7]. On the other hand, conjugation of targeting ligands such as aptamers [8], peptides [9], or DNA [10], also confers nanomaterials with targeting capacity toward microorganisms[11–13]. Different types of microscopy (e.g., TEM, AFM, SEM) and molecular biology techniques offer powerful approaches to probe bacteria-nanomaterials interactions [14–19].

In the present study, we have addressed the interactions between chitosan-based nanocapsules (NC) and an E. coli bearing a synthetic QS genetic circuitry to work as a reporter strain (or biosensor) of bacterial QS [20]. QS is an exquisite chemical-based cell-to-cell communication system that was discovered to operate in bacteria and other microorganisms. QS is regulated by the synthesis of small signaling molecules known as autoinducers (AIs), and by the synthesis of intracellular and membrane proteins that detect the AIs. QS monitors cell population density and plays a critical role in regulating diverse traits and mounting of orchestrated collective behaviors such as biofilm formation, bioluminescence and virulence production [21]. In many Gram-negative bacteria, QS is regulated by acyl-homoserine lactones (AHLs) that vary in the length of the alkyl side chain, or the presence of hydroxyl- or oxo-substituents. Disruption of bacterial QS either using specific inhibitors that compete with or enzymes that degrade AHLs, without exerting toxicity, is considered as a promising approach to circumvent bacterial drug-resistance and a route to the development of a new generation of medicines to deal with bacterial infections [22,23].

Particles produced from inorganic substances such as metals, or silica, ranging in size from a few nanometers to the micrometer length scale, have extensively been studied for their use in antibacterial control [24–26]. Also, particles comprising organic building blocks such as polymers, lipids, or proteins of a different type, have been used to prepare antibiotic-loaded formulations for controlled drug delivery [27–29]. In particular, in the recent years, an increasing number of studies have focused on exploring the impacts of nanomaterials on bacterial QS signaling. [30–33] These have included the study of nanomaterials loaded either with QS inhibitors [34], or with AIs, as well as polymeric materials obtained by molecular imprinting with high recognition capacity to sequester AHLs, and thus inhibit QS responses [35,36].

This study deals with the interaction of chitosan-based nanocapsules (NC) and bacteria. NC can be considered as nano-vesicular systems that contain a reservoir comprised of a liquid oil core stabilized by a surfactant and coated by a polymeric shell such as chitosan (CS). These systems are formed by spontaneous emulsification [37], as first described by Calvo et al. [38]. CS-based NC have become a versatile drug nanocarrier platform, both for lipophilic substances and hydrophilic macromolecules [39–45].

Despite the wealth of studies that have addressed the interaction of bacteria with nanomaterials, there has been a paucity in works addressing the direct interaction of particles with bacteria and the local effect at the bacterial surface. Only recently studies have started to investigate the influence of nanomaterials on the QS response [30,31]. To the best of our knowledge, this, along with an accompanying study [46], are the first studies in their kind that account for the interaction of chitosan-based nanoparticles with an E. coli reporter strain of AHL-mediated QS.

To this end, we have firstly implemented a protocol to estimate the number of chitosan-based NC that bind with E. coli bacteria and found a “stoichiometric” optimum at which NCs and bacteria aggregate, beyond which upon subsequent addition of NCs, they no longer bind to the bacteria. In parallel, we have developed an in silico simulation platform that enabled us to simulate the interactions mediating NC-NC and NC-bacteria, and thus to recreate the experimental results with an extremely reasonable agreement. We have also evaluated the influence of varying numbers of AHL-loaded NCs on the QS response of the E. coli biosensor.

2. Materials and Methods

2.1 Materials

Chitosan of biomedical grade was provided by Mahtani Chitosan Pvt. Ltd., India and was the same sample used in previous studies [47]. The molecular weight of 115 kDa was determined by HPSEC-MALLS and the degree of acetylation of 42 % by ^{1}H-NMR spectroscopy. The characteristics of chitosan were selected, such that they did not inhibit the bacterial growth of the E. coli strain (unpublished); lecithin was a kind gift from Cargill (Epikuron 145 V, Cargill texturing solutions Deutschland GmbH & Co. KG, Hamburg, Germany); Miglyol 812 N was from Sasol GmbH (Witten, Germany); 3OC$_6$HSL and all other chemicals were of analytical grade and were from Sigma-Aldrich Chemie GmbH (Hamburg, Germany).

2.2. Preparation of the nanoformulations

Chitosan-based NC and nanoemulsions (NE) were prepared according to with the protocol developed by Calvo et al. [48] with slight modifications introduced in our recent studies [45]. NE were prepared under an identical protocol but without the addition of chitosan and HCl in the aqueous phase. To prepare different concentrations of 3OC$_6$HSL-loaded NC, 500 µL of an 80 mg/mL ethanolic lecithin solution was mixed with 10 mL of different concentration (10, 20, 40, 60, 120, 200 and 400 nM) ethanolic 3OC$_6$HSL solutions and 125 µL Miglyol 812 N as the organic phase.

2.3 Physical Characterization of nanocapsules and nanoemulsions

2.3.1. Dynamic light scattering with non-invasive back scattering (DLS-NIBS)

The intensity size (hydrodynamic diameter) distributions of the NC and NE were determined by dynamic light scattering with non-invasive back scattering (DLS-NIBS) at 25 °C. A Zetasizer NanoZS instrument (Malvern Instruments Ltd., Worcestershire, UK) equipped with a 4 mW helium/neon laser (λ = 633 nm), and detection was at an angle of 173° was used for these measurements.

2.3.2 Nanoparticle tracking analysis (NTA)

The number size (hydrodynamic diameter) distribution and concentration of NC and NE were determined by nanotracking analysis (NTA) with a NanosSight LM 20 (Malvern Instruments Ltd., Worcestershire, UK), equipped with a laser beam (λ = 640 nm) source. The samples were diluted with MilliQ water, to an acceptable concentration, namely between 10^5 and 10^{10} particles/mL. Each sample was measured in triplicates at 25 °C. Manual shutter and gain adjustments were: Slider shutter 781, slider gain 239 for NC; slider shutter 774, slider gain 161 for NE. The particles were visualized in the sample chamber, and the data was captured and analyzed using the software NTA V3.1.

2.3.4 ζ–potential

The ζ-potential of NC and NE was measured by phase analysis light scattering and mixed laser Doppler velocimetry (M3-PALS) at 25 °C. The samples were diluted 1:100 in 1 mM potassium chloride and analyzed in a Zetasizer NanoZS instrument (Malvern Instruments Ltd., Worcestershire, UK).

2.4 Biological assays

2.4.1. E. coli

E. coli Top10 was chemically transformed with the plasmid pSB1A3-BBa_T9002, carrying the BBa_T9002 genetic device (Registry of Standard Biological Parts: http://parts.igem.org/Part:BBa_T9002), kindly donated by Prof. Anderson Lab (UC Berkeley, USA). A flask with 10mL of Luria Bertani (LB) broth, supplemented with 200 ug/mL ampicillin, was inoculated with a single colony from a freshly streaked plate of strain Top10 pSB1A3 - BBa_T9002. After incubation for 18 h at 37ºC with vigorous shaking, 0.5mL aliquots of the overnight culture were mixed with 0.5mL of 30% glycerol and stored at -80ºC until further usage. The transformed strain is a biosensor that can respond to the N-(3-oxohexanoyl)-L-homoserine lactone ($3OC_6HSL$) and it is the same strain used in accompanying studies [46,49]. The sequence BBa_T9002 comprised the luxR gene, coding for the transcriptional factor LuxR, under the control of the pTetR promoter, being expressed in a constitutive manner. Upon external addition of $3OC_6HSL$, the dimerization of two monomeric species of LuxR, each bound to one AHL molecule, drives to activation of gfp expression through binding of the LuxR-AHL dimerized complex to the lux pR promoter.

2.4.2 Growth media and conditions

Bacterial strains were cultivated using on Luria-Bertani (LB) purchased from Sigma-Aldrich Chemie GmbH (Hamburg, Germany) and M9 minimal medium purchased from Becton, Dickinson and company, Germany. For the following assays (2.4.3. – 2.4.5.), 40 µL of the bacterial glycerol stock were inoculated into 20 mL of LB medium supplemented with 200 µg/mL ampicillin and incubated overnight at 37 °C overnight. The bacterial suspension was washed three times by centrifuging at 4000 rpm for 10 min and resuspended with Milli-Q water. Finally, the suspension was sub-diluted with Milli-Q water to a final OD_{600} = 0.2. 0.2. Prior to biosensor assays (section 2.4.6), 40 µL of the bacterial glycerol stock were inoculated into 20 mL of M9 minimal medium supplemented with 0.5% casamino acids, 1mM thiamine hydrochloride, 0.4% glucose and ampicillin (200 µg/mL) and grown until an OD_{600} between 0.04 and 0.07 (~4 h).

2.4.3. ζ–potential studies

An aliquot of NC or NE suspension of known number of particles per unit volume was added to 1 mL of a bacterial culture of known number of bacteria ($OD_{600} \approx 0.2$, 4.9 x 10^8 CFU/mL) prepared as described above. The culture was incubated at 4 °C and under shaking at 100 rpm for 1 h. The ζ-potential of the suspension was determined by M3-PALS at 25 °C, with a Zetasizer NanoZS instrument (Malvern Instruments Ltd., Worcestershire, UK), as described above.

2.4.4. Quantification of the binding of nanocapsules to bacteria

An aliquot of NC or NE suspension of known number of particles per volume unit was added to 1 mL of a bacterial culture of known number of bacteria ($OD_{600} \approx 0.2$, 4.9*10^8 CFU/mL) prepared as described above. The culture was incubated for 1 h at 4 °C and under shaking at 100 rpm. Under these conditions, no growth was observed. Subsequently, the NC-bacteria suspension was centrifuged for at 4000 rpm for 10 min and the supernatant transferred to a new tube. Varying number ratios of NC/bacterium were explored in these experiments. The number of NC associated with bacteria was determined indirectly from the number of NC in the supernatant which did not interact with bacteria, as determined by DLS-NIBS and the corresponding calibration curve (Fig. S1). The percentage of bound NC (%) is given by

$$NC_{bound}(\%) = \frac{NC_{total} - NC_{free}}{NC_{total}} * 100\% \quad (1)$$

Where, NC_{bound} represents the number of NCs bound to bacteria; NC_{total} and NC_{free} are the number of NC originally added, and the number of NC determined in the supernatant after centrifugation, respectively.

2.4.5. SEM imaging

Aliquots of the NC suspension were mixed with a suspension of bacteria in water ($OD_{600} \approx 0.2$; 4.9 $x10^8$ CFU/mL) to examine different NC/bacterium ratios, namely 36, 72, 109, 362, and 3620. The suspensions were incubated for 1 h at 4 °C under shaking at 100 rpm. Subsequently, the mixtures were vacuum filtered through a track-etched polycarbonate membrane with 1.2 µm pore size. After filtering, the membranes were fixed in 2.5 % aqueous glutaraldehyde for 1 h and washed with PBS once for 10 min after fixing. Finally, the samples were dehydrated through a graded series of aqueous ethanol solutions (10, 30, 50, 70, 90, and 100 % v/v) for 10 min each and kept in a sealed desiccator until complete dehydration. Dilute samples of NC and NE were dropped on a smooth and sterile glass and then kept in a sealed desiccator for two days before SEM imaging. All samples were sputter coated with gold and imaged by SEM (S-3000N, Hitachi, Tokio). Micrographs were recorded digitally.

2.4.6. QS biosensor assay

Cell cultures were grown in M9 minimal medium as explained in section 2.4.2 until an OD_{600} ~ 0.04-0.07. Growth was monitored by measuring the optical density at λ = 600 nm (OD_{600}) on a Microplate Reader Safire F129013 (Tecan, Crailsheim, Germany). The OD_{600} readings were converted to colony forming units (CFU/mL) via a colony counting after plating culture aliquots of known OD_{600} and the construction of the calibration curve shown in Fig. S2. To test for NC-mediated QS inhibition activity, we mixed 10 µL of a 10 nM solution of $3OC_6HSL$ with 10 µL of NC in the wells of a flat-bottomed 96-well plate (Greiner Bio-One, cat. # M3061) and each well was then filled with 180 µL aliquots of the bacterial culture. In a different series of experiments, we tested the ability of the NC to deliver the $3OC_6HSL$ to the bacteria. $3OC_6HSL$ was loaded to the organic phase of the NC so as to achieve final AHL concentrations of 10, 20, 40, 60, 120, 200 and 400 nM. In both experiments, bacteria were incubated with different initial NC/bacterium

ratios, namely 2213, 1106, 553, 368, 184, 110 and 55 NC/bacterium, respectively. Different initial NC/bacterium ratios and concentrations of AHL-loaded NC were chosen to ensure that the final concentration of 3OC6HSL in the microplate wells was always 10 nM. Three blank wells with 200 μL of medium were used to measure the absorbance background. Additionally, three control wells containing 180 μL of culture and 20 μL of water were prepared to measure the fluorescence background. The plates were incubated in a Tecan Safire F129013 Microplate Reader (Tecan, Crailsheim, Germany) at 37 °C and fluorescence (λ_{ex} = 480 nm and λ_{em} = 510 nm) and absorbance (OD_{600}) were measured in intervals of 6 min. For each experiment, the fluorescence intensity and OD_{600} data were corrected by subtracting the values of absorbance and fluorescence backgrounds and expressed as the average for each treatment.

2.5. In silico simulation of nanocapsules and bacteria

The simulation was implemented in a set of Python (www.python.org) modules that allow a flexible use of all functions and classes. All python modules and a compiled version for Windows can be downloaded from www.wwu.de/Biologie.IBBP/aggoycoolea/software/. The implementation relies on two open-source python modules, namely numpy for numerical operations, and vpython for graphical representation. NC and bacteria were simulated via a coarse-grained molecular dynamics in a way that particles and bacteria were treated as single solid entities with a center of mass and previously determined dimensions (see Table 2). To this end, a randomized set of initial positions (and velocities) for bacteria and nanoparticles was defined. The evolution of the system with time was determined by the potential "landscape", for which we use the interactions described by Elimelech et al [50]. To simplify the interactions, we considered the nanoparticles as spheres and the bacteria as plates while describing the interaction potentials. The position was determined by the pairwise interaction between NC, bacteria, and between NC and bacteria. The interaction potentials ($U_{ij;T}$, $U_{ij;R}$, and $U_{ij;A}$, equation 22) were calculated between NC according to sphere-sphere interactions for spheres with different radii (r), between bacteria according to plate-plate interaction, and between bacteria and NC according to sphere-plate interactions [50]. The potential was differentiated with respect to the distance to obtain the force that is acting on an entity. NC were subjected to a random force (F_i) proportional to their size, mass (m_i), and viscosity of the medium ($F_{i;R}$). Random movement (corresponding to thermal motion) of bacteria was realized by multiplying the axis vector of a bacterium with a

rotation matrix for a random angle α in front of the bacterium. Both, bacteria and NC were subjected to frictional forces ($F_{i;f}$) as interaction with the thermostat of the system (equation 3). Dividing the force acting on an entity by its mass (m_i) gives the acceleration (a_i) (equation 44). The position was calculated through the Verlet-algorithm that integrates the position via an intermediate velocity ($V_{i;t}$) (equations 55-77). See Figure 5Sb for a description of the spatial variance of the interaction potentials and forces. Simulations were run for a total of 2 x 10^6 simulation steps which were equivalent to 2 ms real time (time step Δt = 1 ns). The rest of the parameters and their values used in the simulations are shown in Table 2.

The governing equations of the simulation can be described as follows:

$$U_{ij;T} = U_{ij;R} + U_{ij;A} \quad (2)$$

$$F_i(r) = \left(\sum_{j=1, j!=i}^{N} -\frac{dU_{ij;T}}{dr_j}\right) + F_{i;random} + F_{i;friction} \quad (3)$$

$$a_i = \frac{F_i}{m_i} \quad (4)$$

$$V_{i;t+0.5\Delta t} = V_{i;t} + 0.5 a_{i;t} \Delta t \quad (5)$$

$$V_{i;t+\Delta t} = V_{i;t+0.5\Delta t} + a_{i;t+\Delta t} \Delta t \quad (6)$$

$$x_{i;t+\Delta t} = x_{i;t} + V_{i;t+0.5\Delta t} \Delta t \quad (7)$$

Where,

$U_{ij;T}$ = Total interaction potential energy between particles i and j

$U_{ij;R}$ = Repulsive interaction potential energy between particles i and j

$U_{ij;A}$ = Attractive interaction potential energy between particles i and j

$F_i(r)$ = Total force acting on particle i

$F_{i;random}$ = Random force acting on particle i

$F_{i;friction}$ = Frictional force acting on particle i

$a_i(r)$ = Total acceleration of particle i ;

m_i = Mass of particle i

$x_{i;t}$ = Value of quantity x (x = V for velocity and x = a for acceleration) for particle i at time t

Δt = Time step

3. Result and Discussion

3.1 Characterization of chitosan-based nanocapsules and nanoemulsions

The physical characteristics of the NC and NE, namely the size distribution, ζ-potential, and morphology, were investigated by different techniques. SEM images of NC and NE in Figure 1a and 1b, revealed the presence of spherical particles with sizes of <~200 nm. The fact that much better quality of SEM images could be obtained for NC than NE may stem from the fact that a harder shell is expected to occur on the chitosan-coated NC than in the pristine surface of the NE containing only lecithin surfactant.

Table 1 summarizes the physical characterization parameters for both systems. Notice that in the case of NC, the Z-average diameter value (~155 nm) determined by dynamic light scattering with non-invasive back scattering (DLS-NIBS) is somewhat greater than the value (~114 nm) obtained by nanotracker analysis (NTA). The difference is also evident in the combined intensity scattering and number particle size distribution patterns (Figure 1c) determined by one each technique, respectively. The average diameter values agree reasonably well with those reported in previous studies for both types of systems [39]. The distributions observed in both curves reveal the presence of predominantly one population of particles. In the case of DLS-NIBS, though, the presence of a skewed shoulder corresponding to a fraction of particles of larger size (~200-~400 nm) can be noticed. Though much weaker, this shoulder is also noticed in the NTA distribution curve. In the case of NE, a very close agreement was observed between the average size values and both type of distribution curves (cf. Table 1 and Figure 1d), even though a small shoulder corresponding to a fraction of particles of larger size is also evident in both curves. DLS-NIBS and NTA are complementary techniques that enable to obtain a detailed picture of the particle size distribution. DLS-NIBS measures the relative distribution of particle size on the population. The contribution to the scattering intensity of the larger particles is much more predominant than that of the smaller ones. By contrast, NTA records and measures the trajectories of single particles resulting from the scattered light when illuminated by a laser beam. Therefore, NTA affords the absolute number distribution directly, and hence, it is less prone to the influence of the larger particles than DLS-NIBS [51,52]. As expected, the ζ–potential value of NC was highly positive, in direct contrast to the highly negative one of NE devoid of a chitosan shell. Both ζ–potential values were also in close agreement with those obtained in our previous studies [39,53]. As representative of the experimental physical characteristics of the NC, in the in

silico simulation studies discussed below, we used values of 150 nm and +50 mV for the diameter and ζ–potential, respectively.

3.2 Effect of nanocapsules and nanoemulsions on the ζ–potential of the bacteria

A variable known number of NC or NE per unit volume was applied to a known number of bacteria per unit volume, such that the ratio of NC or NE/bacterium varied in the range from 36 to 3620. The ζ–potential of these systems was measured after incubation for 1 h at 4 ºC. Figure 2a shows that the bacteria alone have a negative ζ-potential of ~-50 mV and that upon addition of an increasing number of positively charged NC, it increased and reversed from negative to positive values. This experiment also enabled to determine that at a ratio of ~80 NC/bacterium the ζ–potential is equal to neutral. We denoted this "stoichiometric" NC/bacterium ratio as the "K_m" value, as explained in further detail below. In turn, the ζ–potential of the mixtures of bacteria and NE were highly negative (~ -50 mV), and remained unchanged regardless of the number of added NE (Fig. 2a).

The influence of the varying concentration of NC on the ζ–potential of bacteria offered the first line of experimental evidence of the interaction of NC with the bacterial cell wall. Similar results have been obtained for the attachment of silver nanoparticles on Pseudomonas chlororaphis in other studies [54]. The fact that the negative electrical surface charge of bacteria becomes neutralized and eventually reversed into a positive value, along with the fact that NE had no influence on the ζ–potential of bacteria, argues strongly in favor that electrostatic interactions are the dominant mechanism at play driving the attachment of NC at the bacterial surface.

3.3. Sedimentation studies of the interaction of nanocapsules with bacteria

To further address the problem of the quantitative estimation of the number of NC that interact per bacterium, we used the sedimentation assay. A known number of NC was incubated with a fixed number of bacteria at 4 ºC for 1 h. Under such conditions, the cellular division was assumed to be negligible and hence, the number of bacteria remained unchanged during the assay. After the incubation, the NC-bacteria suspensions were centrifuged, and the NC-bacteria complex formed a solid pellet at the bottom of the tube, while free NC which did not interact with bacteria, remained in the supernatant, as they contain an oil core and are less dense than water [55]. Figure 2b and 2c shows the results of this experiment along with those of the in silico simulation studies. NC/bacterium ratios ranging from 36 to 3620 were investigated. Close inspection of the

experimental trace in Figure 2b shows that up to a value of ~80 NC/bacterium the percentage fraction of NC bound to bacteria (NC_{bound}) was 100 %. Beyond this value, NCs start to be detected in the supernatant upon centrifugation, thus reducing the NC_{bound}. When the data are expressed as the absolute number of bound NC (Figure 2c), it can also be realized that a number of bound NC attains a maximal value of ~80 NC/bacterium when up to 100 NC/bacterium are added. Beyond this, fewer NC seem to attach to the bacteria. Notice also that at 109 NC/bacterium data point, the largest error bar is observed. Visual inspection of the NC-bacteria suspensions revealed that at these concentrations of added NC, large aggregates were formed (See Figure S4). It was also observed that at greater concentrations of NC, the resulting suspensions appeared more turbid without the presence of visible aggregates. Interestingly, the measured ratio of ~80 NC/bacterium up to which the NC_{bound} is 100%, matches exactly that of the attainment of electro neutrality from ζ–potential measurements, designated as K_m (Figure 2a). The experimental evidence of the sedimentation studies is consistent with the fact that a finite number of NC interact at the surface of bacteria, under a precise, specific binding "stoichiometry".

3.4. In silico simulations of the interactions of nanocapsules and bacteria

NC interactions were simulated using an in silico platform that enabled to calculate their surface interaction potentials as well as their Brownian motion. To this end, we used average representative values of diameter (150 nm) and ζ–potential (+50 mV). The resulting behavior of the simulated particles obeyed DLVO theory (see Figure S5). At a surface-to-surface distance of ~43 nm the interaction potential between two particles showed a local minimum of $\phi_{min} = -1.58 \times 10^{-2}\ k_BT$. At lower separation distances of 0.3 nm, there is an energy barrier with $\phi_{max} = 143\ k_BT$, indicating that at lower separation distances, attractive forces exceed repulsive ones, and particles may aggregate. When the potential is differentiated with respect to the separation distance, the forces acting on the particles can be obtained. As can be seen in Figure S5B, the repulsive forces at the energy barrier are in the order of 10^{-10} N, whereas random forces due to Brownian motion are in the range of 10^{-11} N. This means that under the simulated conditions, the system will remain stable since the random forces cannot overcome the energy barrier. Remarkably, in dilute conditions at separation distances greater than the particle diameter, the interaction forces are five orders of magnitudes smaller than the random forces. In turn, this also means that NC are not actively attracted by bacteria. It is rather the case that

particles occasionally come nearby of the bacterial surface due to Brownian motion until a point where the attractive forces dominate, and particles collide on the bacterial surface.

We simulated different NC/bacterium ratios in suspension to assess similar conditions as those shown in Figure 2b and 2c. A similar trend was observed regardless of whether we simulated a single bacterium or an ensemble of three bacteria in the same volume (Fig. 2b). Notice that the results from the simulations are in remarkable close agreement to the experimentally obtained data in the sense that the point of which less than 100 % of the applied particles remain bound to the bacterium matches the ~80 NC/bacterium ratio. At greater NC/bacterium ratios, the simulated data curves deviate from the experimental one, by predicting greater values of NC_{bound}. This deviation might be a result of the used experimental isolation protocol. When NC are subjected to gravitational force during centrifugation, they do not sediment due to their lower density than water (in fact, at sufficiently high speeds they undergo phase separation and form a creamy layer on the top). It is possible, that during centrifugation process some NC might have detached from the bacterial surface and subsequently appear in the supernatant, thus predicting an underestimated percentage of interaction [56].

While the experimental results only give conclusive evidence on the number of NC that interact with one bacterium up to point where NC_{bound} decreases from 100 %, the simulation provides more information at higher ratios. Although the percentage of interaction decreases above a NC/bacterium ratio of ~80, when the data are expressed as the absolute number of particles attached to the bacterial surface, the value increases steadily and reaches a maximum of 145 (Figure 2c). Fitting the absolute number NC vs. the ratio of NC/bacterium to a Hill function afforded very high $R^2 \geq 0.99$. This treatment yields a maximum number of NC that interact with one bacterium of 145 and a half maximum value, $K_m = 78$. This K_m value matches almost exactly with the measured value of the number of attached NC before a decrease in NC_{bound} starts to decrease (Figure 2b), as well as that when electrical neutrality was observed (Figure 2a). A value of $n = 1.53$ for the cooperativity constant in the Hill equation suggests that upon binding of one particle, the likelihood for another particle to bind increases.

In the performed simulations, for a separation distance of 32 nm between two particles bound at the bacterial surface the effective angle occupied by one particle is $\beta = 22°$ (for the detailed calculations see supporting information). At this distance, the total number of particles around one bacterium is 145 suggesting that at the saturation point obtained from in silico simulations the distance between two particles is on average 32 nm.

3.5. SEM imaging of bacteria mixed with nanocapsules

The interaction of NC and bacteria was further investigated by SEM imaging (Figure 3b-f). As we have shown before, NC interact with bacteria up to a "stoichiometric" half-maximal value K_m = 78 NC/bacterium. SEM images were obtained at lower and greater NC/bacterium ratios than this value. Figure 3a shows the image of E. coli bacteria alone, revealing the presence of isolated bacteria with a smooth surface. However, even at the lowest concentration of added NC, the bacteria appear as conglomerates of fused cells as can be seen in Figure 3b, 3c, and 3e. This is particularly evident in Figure 3c that shows a magnified image of one bacterium. Notice that the bacterial surface does not appear as smooth as in the pristine cells (cf. Figure 3a and d), but reveals the presence of small protrusions leaving out of the cell wall. Also, the presence of at least one NC is evident. The presence of protrusions can be explained as a disruption of the cell wall once the NC are attached and inserted into the cell membrane, which can lead to an increase of the fluidity and leakage of cell contents [4]. Figure 3f shows that at a large excess number of NC, bacteria appear disaggregated. Probably this is because at such large density of NC, the bacterial surface becomes oversaturated with NC, in keeping with the results predicted by in silico simulations. The high positive charge of NC and possibly other effects at play, seem to prevent the formation of conglomerates and to drive the exclusion of individual bacteria [57].

3.6. Effect of nanocapsules on the bacterial quorum sensing activity,

To test the influence of the number of NC and of the bacteria-NC aggregation (as evidenced by SEM) on the QS activity, blank NC, and $3OC_6HSL$-loaded NC were applied to the biosensor assay at different initial NC/bacterium ratios, namely 55, 110, 184, 368, 553, 1107 and 2213. The first interesting finding from these assays was that the treatment of bacteria with blank or $3OC_6HSL$-loaded NC did not inhibit bacterial growth in the time course of the assay during 360 min (Figure 4a and 4b). Also, it is possible to notice that at specific ratios, namely 184 and 368 NC/bacterium, the OD_{600} traces for both blank and $3OC_6HSL$-loaded NC showed a sudden increase. By contrast with the NC-bacteria interaction studies described earlier, in which the incubation of NC and bacteria was conducted at 4 ºC hence the bacterial growth was inhibited, in the QS assays, the bacteria were growing, and hence, the NC/bacterium ratios decreased in the course of the experiment (see Figure S7). The sudden "bumps" observed in the growth traces, centered at ~200 min can be explained as the consequence of attaining specific NC/bacterium

ratios that result in the sudden aggregation of the colonies, and thus in the increase in OD_{600} values. Our SEM and sedimentation results are consistent with the notion of the existence of an optimal "stoichiometric" ratio of NC/bacterium of ~80 at which the electrical charge of bacteria and NC is fully compensated (i.e., ζ–potential ~ 0) and the bacteria form large conglomerates (Figure S4). Interestingly, the "bumps" in OD_{600} were only observed when the initial NC/bacterium ratios were either 368 or 184, and not at any other initial ratios. It seems that only in these two cases, the optimal stoichiometric ratio was hit in the course of growth while in the rest of the cases, it was not.

Figure 4a and 4b also shows the QS response of the E. coli biosensor, as quantified by the fluorescence intensity associated with the overexpression of the GFP reporter gene, once it is induced by $3OC_6HSL$. The first striking fact to notice is that regardless of whether the $3OC_6HSL$ is loaded into the NC or added externally (as in the case of blank NC), the fluorescence response is induced, albeit attenuated with respect to the control. A detailed inspection of the fluorescence intensity traces, though, reveals a rather peculiar dependence of the GFP expression on the concentration of added NC. In the case of blank NC, notice that a progressive reduction in the fluorescence ensues after ~200 min at the low ratios of 55, 110, 184 NC/bacterium. At greater ratios, the attenuation in fluorescence intensity starts at ~275 min. In the case of $3OC_6HSL$-loaded NC, the fluorescence intensity traces describe a remarkably comparable pattern as for the blank NC ones. Again, the minimal fluorescence intensity end-point values are registered at the lower concentrations of NC/bacterium (55 - 184 NC/bacterium), and beyond this point, an increase in the concentration of NC results in the gradual increase in the fluorescence intensity. Figure 4c summarizes the QS inhibition rates. Worth of notice is the extremely close agreement of the two traces, despite the apparent different conditions.

Nanoparticles have gained enormous traction in the past two decades as broad-spectrum antimicrobial agents [58]. However, an increasing number of recent studies are being centered mostly on inorganic nanoparticles to inhibit the bacterial QS activity. Recently, ZnO nanoparticles have been tested against six clinical bacterial strains of Pseudomonas aeruginosa and found that they decreased the virulence production and biofilm formation for most of the strains [59]. Several mechanisms have been proposed for the inhibition of bacterial QS activity, Naik et al. evaluated AgCl-TiO_2 nanoparticles with Chromobacterium violaceum for their anti-QS activity, their studies confirmed that the inhibition of violacein production was due to AHL inhibition while not repressing bacterial growth [32]. Mohanty et al. quantified the influence of

silver nanoparticles and single-wall carbon nanotubes on the reduction of the AHL synthesis and revealed that the effects of nanomaterials on QS signaling are highly dependent on bacterial species [30]. Another mechanism of QS inhibition activity of nanoparticles is by adsorption of AHLs to nanoparticles. For example, functionalized silicon dioxide nanoparticles were designed to carry *β*-cyclodextrin that bind AHLs, thus removing this signal molecules from the immediate bacterial environment [31].

Our study with the AHL-sensitive E. coli biosensor strain shows that NC can considerably reduce the expression of GFP and this is mostly achieved when the number of added NC is close to the "stoichiometric" ratio of NC/bacterium that compensates the electrical charge of the cell wall of bacteria and induces their aggregation. This effect was confirmed in two different scenarios, namely when the AHL were added directly to the culture medium, or when they were loaded into the core of the NC.

The observed greatest inhibition in the QS response could be explained as the restriction imposed on the diffusion of AHL as the bacteria are driven to aggregation by NC. Previous studies explain that bacterial biofilms form as 'microcolonies', and the development is a complex process [60]. In fact, even suspended aggregates of cells display many of the characteristics that are associated with biofilms [61]. The E. coli bacteria in our experiments aggregated and seemed to form 'microcolonies' upon adding NC at a very narrow range of concentration, equivalent to 36 - 72 NC/bacterium (Figure S4). As we explained above, in the biological assays of QS activity, the bacterial growth increases in the course of the duration of the assay, while the NC number keeps constant, with the consequent decrease in the ratio of NC/bacterium (Fig. S6). Our experiments show that when NC are dosed at low NC/bacterium ratios (55 - 184) the onset of the attenuation of GFP expression occurs at ~200 min, this is probably the time point at which aggregation is maximized. Such aggregation is likely to impose a restriction on the diffusion of $3OC_6HSL$ to the cell. At the higher NC/bacterium ratios (368 - 2213) the attenuation of GFP expression only starts at ~270 min. At such conditions, much over the NC/bacterium stoichiometric ratio, it takes longer for the number of bacteria to reach the optimal ratio to drive bacteria into aggregation.

When the $3OC_6HSL$ is loaded into the NCs, two possible explanations can be offered to the observed effects on the QS fluorescence output response. The first is that the $3OC_6HSL$ is burst released from the NCs to the medium as soon as they are diluted. Released $3OC_6HSL$ out of the NC would diffuse to the cell, very much in a similar way when it is added in the free form. This

would explain the close similarity of the inhibition rates for both scenarios (Figure 4c). A second possibility would be that the $3OC_6HSL$ is released locally at the cell membrane and directly into the cytosol. At the moment, we do not have enough experimental evidence to favor unequivocally either of these mechanisms.

4. Conclusion

In this study, we have demonstrated both experimentally and in silico that chitosan-based NC bind to E. coli bacteria in a quantitative manner. This interaction can be explained by DLVO theory, accounting for the attractive and repulsive components that determine the total potential force. Upon binding at a "stoichiometric" NC/bacterium ratio of ~80, the surface charge of bacteria-NC complex is compensated, and bacteria appear forming large conglomerates. Our experiments are consistent with the notion that NC can interact with E. coli driven by an electrostatic interaction. The main significance of these results lies in the following: 1) Chitosan-coated NC are non-toxic, even when they promote the aggregation of E. coli when added at a very narrow range of concentration; 2) NC themselves can inhibit the "hearing" or "sensing" component of bacterial QS; 3) In the same manner that $3OC_6HSL$ was loaded into the oil core of NC, and it was delivered effectively to bacteria to trigger their QS response, it should be feasible to load compounds with QS inhibitory activity, such as cinnamaldehyde [62,63] and other.

Acknowledgements

XQ was recipient of a fellowship from China Scholarship Council. CVS was supported by a pre-doctoral fellowship of the Xunta de Galicia and by a FPU fellowship of the "Ministerio de Educación y Ciencia" of Spain, by a research fellowship of DAAD (Germany), and a research fellowship of the Fundación Pedro Barrié de la Maza (Spain). SD was recipient of a fellowship from the "WISE" Programme of DAAD (Germany). We acknowledge support from The Danish Agency for Science, Technology and Innovation, Denmark (FENAMI project 10-093456); the research leading to these results has also received funding from the European Union's Seventh Framework Programme for research, technological development and demonstration under grant agreement no. 613931. We are indebted to Antje von Schaewen for the generous access to the Safire Tecan-F129013 Microplate Reader, and to Prof. Martin Wiemann for access and support in the NTA determinations.

References

[1] C. Sousa, D. Sequeira, Y. V. Kolen'Ko, I.M. Pinto, D.Y. Petrovykh, Analytical protocols for separation and electron microscopy of nanoparticles interacting with bacterial cells, Anal. Chem. 87 (2015) 4641–4648. doi:10.1021/ac503835a.

[2] C.O. Dimkpa, A. Calder, P. Gajjar, S. Merugu, W. Huang, D.W. Britt, J.E. McLean, W.P. Johnson, A.J. Anderson, Interaction of silver nanoparticles with an environmentally beneficial bacterium, Pseudomonas chlororaphis, J. Hazard. Mater. 188 (2011) 428–435.

[3] K. Forier, K. Raemdonck, S.C. De Smedt, J. Demeester, T. Coenye, K. Braeckmans, Lipid and polymer nanoparticles for drug delivery to bacterial biofilms, J. Control. Release. 190 (2014) 607–623. doi:10.1016/j.jconrel.2014.03.055.

[4] M.M. Fernandes, A. Francesko, J. Torrent-burgue, F.J. Carrio, T. Heinze, T. Tzanov, Sonochemically Processed Cationic Nanocapsules: Efficient Antimicrobials with Membrane Disturbing Capacity, Biomacromolecules. 15 (2014) 1365−1374.

[5] L. Qi, Z. Xu, X. Jiang, C. Hu, X. Zou, Preparation and antibacterial activity of chitosan nanoparticles, Carbohydr. Res. 339 (2004) 2693–2700. doi:10.1016/j.carres.2004.09.007.

[6] Z.V. Feng, I.L. Gunsolus, T.A. Qiu, K.R. Hurley, L.H. Nyberg, H. Frew, K.P. Johnson, A.M. Vartanian, L.M. Jacob, S.E. Lohse, M.D. Torelli, R.J. Hamers, J. Murphy, C.L. Haynes, Impacts of gold nanoparticle charge and ligand type on surface binding and toxicity to Gram- negative and Gram-positive bacteria, Chem. Sci. 6 (2015) 5186–5196. doi:10.1039/C5SC00792E.

[7] M. Grodzik, P. Orlowski, A. Sokolowska, Visualization of interaction between inorganic nanoparticles and bacteria or fungi, Int. J. Nanomedicine. 5 (2010) 1085–1094. doi:10.2147/IJN.S13532.

[8] Y. Chang, C.-Y. Yang, R. Sun, Y. Cheng, W. Kao, P. Yang, Rapid single cell detection of

Staphylococcus aureus by aptamer-conjugated gold nanoparticles, Sci. Rep. 3 (2013) 1–7. doi:10.1038/srep01863.

[9] D. Akin, J. Sturgis, K. Ragheb, D. Sherman, K. Burkholder, J.P. Robinson, A.K. Bhunia, S. Mohammed, R. Bashir, Bacteria-mediated delivery of nanoparticles and cargo into cells, Nat. Nanotechnol. 2 (2007) 441–449. doi:10.1038/nnano.2007.149.

[10] Q. Hu, M. Wu, C. Fang, C. Cheng, M. Zhao, W. Fang, P.K. Chu, Y. Ping, G. Tang, Engineering Nanoparticle-Coated Bacteria as Oral DNA Vaccines for Cancer Immunotherapy, Nano Lett. 15 (2015) 2732–2739. doi:10.1021/acs.nanolett.5b00570.

[11] L. Zhang, D. Pornpattananangkul, C.J. Hu, C. Huang, Development of Nanoparticles for Antimicrobial Drug Delivery, Curr. Med. Chem. 17 (2010) 585–594.

[12] P. Tallury, A. Malhotra, L.M. Byrne, S. Santra, Nanobioimaging and sensing of infectious diseases, Adv. Drug Deliv. Rev. 62 (2010) 424–437. doi:10.1016/j.addr.2009.11.014.

[13] B. Kim, W. Yang, J. Ryu, Y. Yoo, M. Lee, Carbohydrate-coated nanocapsules from amphiphilic rod–coil molecule: binding to bacterial type 1 pili, Chem. Commun. (2005) 2035–2037. doi:10.1039/B419258C.

[14] I. Armentano, C.R. Arciola, E. Fortunati, D. Ferrari, S. Mattioli, C.F. Amoroso, J. Rizzo, J.M. Kenny, M. Imbriani, L. Visai, The Interaction of Bacteria with Engineered Nanostructured Polymeric Materials : A Review, Sci. World J. (2014) Article ID 410423.

[15] D.A. Pelletier, A.K. Suresh, G.A. Holton, C.K. Mckeown, W. Wang, B. Gu, N.P. Mortensen, D.P. Allison, D.C. Joy, M.R. Allison, S.D. Brown, T.J. Phelps, M.J. Doktycz, A.P.P.L.E.N.M. Icrobiol, Effects of Engineered Cerium Oxide Nanoparticles on Bacterial Growth and Viability, Appl. Environ. Microbiol. 76 (2010) 7981–7989. doi:10.1128/AEM.00650-10.

[16] J.R. Morones, J.L. Elechiguerra, A. Camacho, K. Holt, J.B. Kouri, J.T. Ram, M.J. Yacaman, The bactericidal effect of silver nanoparticles, Nanotechnology. 16 (2005) 2346–2353. doi:10.1088/0957-4484/16/10/059.

[17] J. Crespo, J. Garcı, C. Torres, M.E. Olmos, Y. Sa, Organometallic approach to polymer-protected antibacterial silver nanoparticles : optimal nanoparticle size-selection for bacteria interaction, J Nanopart Res. 14 (2012) 1281. doi:10.1007/s11051-012-1281-y.

[18] S.C. Hayden, G. Zhao, K. Saha, R.L. Phillips, X. Li, O.R. Miranda, V.M. Rotello, M.A. El-Sayed, I. Schmidt-Krey, U.H.F. Bunz, Aggregation and interaction of cationic nanoparticles on bacterial surfaces, J. Am. Chem. Soc. 134 (2012) 6920–6923.

doi:10.1021/ja301167y.

[19] I. Gammoudi, N.R. Faye, F. Moroté, D. Moynet, C. Grauby-heywang, Characterization of Silica Nanoparticles in Interaction with Escherichia coli Bacteria, Int. J. Chem. Mol. Nucl. Mater. Metall. Eng. 7 (2013) 520–526.

[20] C. Vila-Sanjurjo, C. Engwer, X. Qin, L. Hembach, T. Verdía-Cotelo, C. Remuñán-López, A. Vila-Sanjurjo, F. M. Goycoolea. A single intracellular protein governs the critical transition from an individual to a coordinated population response during quorum sensing: Origins of primordial language. bioRxiv 074369; doi:http://dx.doi.org/10.1101/074369 (Jump line).

[21] H.D. Lu, A.C. Spiegel, A. Hurley, L.J. Perez, K. Maisel, L.M. Ensign, J. Hanes, B.L. Bassler, M.F. Semmelhack and R.K. Prud. Modulating Vibrio cholerae quorum-sensing-controlled communication using autoinducer-loaded nanoparticles, Nano Lett. 15, 2015, 2235–2241, http://dx.doi.org/10.1021/acs.nanolett.5b00151..

[22] B. LaSarre, M.J. Federle, Exploiting Quorum Sensing To Confuse Bacterial Pathogens, Microbiol. Mol. Biol. Rev. 77 (2013) 73–111. doi:10.1128/MMBR.00046-12.

[23] V.C. Kalia, Quorum sensing inhibitors : An overview, Biotechnol. Adv. 31 (2013) 224–245. doi:10.1016/j.biotechadv.2012.10.004.

[24] M.J. Hajipour, K.M. Fromm, A. Akbar Ashkarran, D. Jimenez de Aberasturi, I.R. De Larramendi, T. Rojo, V. Serpooshan, W.J. Parak, M. Mahmoudi, Antibacterial properties of nanoparticles, Trends Biotechnol. 30 (2012) 499–511. doi:10.1016/j.tibtech.2012.06.004.

[25] K. Markowska, A.M. Grudniak, K.I. Wolska, Silver nanoparticles as an alternative strategy against bacterial biofilms, Acta Biochim. Pol. 60 (2013) 523–530.

[26] C.A. Strassert, M. Otter, R.Q. Albuquerque, A. Hone, Y. Vida, B. Maier, L. De Cola, Photoactive hybrid nanomaterial for targeting, labeling, and killing antibiotic-resistant bacteria, Angew. Chemie - Int. Ed. 48 (2009) 7928–7931. doi:10.1002/anie.200902837.

[27] A.N. Brown, K. Smith, T.A. Samuels, J. Lu, S.O. Obare, M.E. Scott, Nanoparticles Functionalized with Ampicillin Destroy Multiple- Antibiotic-Resistant Isolates of Pseudomonas aeruginosa and Enterobacter aerogenes and Methicillin-Resistant Staphylococcus aureus, Appl. Environ. Microbiol. 78 (2012) 2768–2774. doi:10.1128/AEM.06513-11.

[28] R. Díez-Martínez, E. García-Fernández, M. Manzano, Á. Martínez, M. Domenech, M.

Vallet-Regí, P. García, Auranofin-loaded nanoparticles as a new therapeutic tool to fight streptococcal infections, Sci. Rep. 6 (2016) 19525. doi:10.1038/srep19525.

[29] A.M. Piras, G. Maisetta, S. Sandreschi, M. Gazzarri, C. Bartoli, L. Grassi, S. Esin, F. Chiellini, G. Batoni, Chitosan nanoparticles loaded with the antimicrobial peptide temporin B exert a long-term antibacterial activity in vitro against clinical isolates of Staphylococcus epidermidis, Front. Microbiol. 6 (2015) 1–10. doi:10.3389/fmicb.2015.00372.

[30] A. Mohanty, C.H. Tan, B. Cao, Impacts of nanomaterials on bacterial quorum sensing: differential effects on different signals, Environ. Sci. Nano. 3 (2016) 351–356. doi:10.1039/C5EN00273G.

[31] K.P. Miller, L. Wang, Y. Chen, P.J. Pellechia, B.C. Benicewicz, A.W. Decho, Engineering nanoparticles to silence bacterial communication, Front. Microbiol. 6 (2015). doi:10.3389/fmicb.2015.00189.

[32] K. Naik, M. Kowshik, Anti-quorum sensing activity of AgCl-TiO2 nanoparticles with potential use as active food packaging material, J. Appl. Microbiol. 117 (2014) 972–983. doi:10.1111/jam.12589.

[33] A. Gupta, J.L. Terrell, R. Fernandes, M.B. Dowling, G.F. Payne, S.R. Raghavan, W.E. Bentley, Encapsulated Fusion Protein Confers “‘ Sense and Respond ’” Activity to Chitosan – Alginate Capsules to Manipulate Bacterial Quorum Sensing, Biotechnol. Bioeng. 110 (2013) 552–562. doi:10.1002/bit.24711.

[34] N. Nafee, A. Husari, C.K. Maurer, C. Lu, C. De Rossi, A. Steinbach, R.W. Hartmann, C. Lehr, M. Schneider, Antibiotic-free nanotherapeutics: Ultra-small, mucus-penetrating solid lipid nanoparticles enhance the pulmonary delivery and anti-virulence efficacy of novel quorum sensing inhibitors, J. Control. Release. 192 (2014) 131–140. doi:10.1016/j.jconrel.2014.06.055.

[35] E. V Piletska, G. Stavroulakis, K. Karim, M.J. Whitcombe, I. Chianella, A. Sharma, K.E. Eboigbodin, G.K. Robinson, Attenuation of Vibrio fischeri Quorum Sensing Using Rationally Designed Polymers, (2010) 975–980.

[36] E. V Piletska, G. Stavroulakis, L.D. Larcombe, M.J. Whitcombe, A. Sharma, S. Primrose, G.K. Robinson, S.A. Piletsky, Passive Control of Quorum Sensing : Prevention of Pseudomonas aeruginosa Biofilm Formation by Imprinted Polymers, Biomacromolecules. 12 (2011) 1067–1071.

[37] J.C. López-montilla, P.E. Herrera-morales, S. Pandey, D.O. Shah, J.C. Lopez-montllta, P.E. Herrera-morales, S. Pandey, D.O. Shah, Spontaneous Emulsification : Mechanisms , Physicochemical Aspects , Modeling , and Applications, Dispers. Sci. Technol. 23 (2002) 219–268. doi:10.1080/01932690208984202.

[38] C.R.-L. P. Catvo, M.J.A. J.L, Vila-Jato, Development of positively charged colloidal drug carriers : chitosan-coated polyester nanocapsules and submicron-emulsions, Colloid Polym. Sci. 275 (1997) 46–53.

[39] F.M. Goycoolea, A. Valle-gallego, R. Stefani, B. Menchicchi, L. David, C. Rochas, M.J. Santander-ortega, M.J. Alonso, Chitosan-based nanocapsules : physical characterization , stability in biological media and capsaicin encapsulation, Colloids Surfaces B Biointerfaces. 2 (2012) 1423–1434. doi:10.1007/s00396-012-2669-z.

[40] C. Prego, M. Garcia, D. Torres, M.J. Alonso, Transmucosal macromolecular drug delivery, J. Control. Release. 101 (2005) 151–162. <Go to ISI>://000226086800014.

[41] M. V. Lozano, D. Torrecilla, D. Torres, A. Vidal, F. Domínguez, M.J. Alonso, Highly efficient system to deliver taxanes into tumor cells: Docetaxel-loaded chitosan oligomer colloidal carriers, Biomacromolecules. 9 (2008) 2186–2193. doi:10.1021/bm800298u.

[42] C. Prego, D. Torres, M.J. Alonso, Chitosan nanocapsules as carriers for oral peptide delivery: Effect of chitosan molecular weight and type of salt on the in vitro behaviour and in vivo effectiveness, J. Nanosci. Nanotechnol. 6 (2006) 2921–2928. <Go to ISI>://000240865900032.

[43] S. Vicente, M. Peleteiro, B. Díaz-Freitas, A. Sanchez, Á. González-Fernández, M.J. Alonso, Co-delivery of viral proteins and a TLR7 agonist from polysaccharide nanocapsules: a needle-free vaccination strategy., J. Control. Release. 172 (2013) 773–781.

[44] S. Vicente, B. Diaz-Freitas, M. Peleteiro, A. Sanchez, D.W. Pascual, A. Gonzalez-Fernandez, M.J. Alonso, A Polymer/Oil Based Nanovaccine as a Single-Dose Immunization Approach, PLoS One. 8 (2013) 2–9. doi:10.1371/journal.pone.0062500.

[45] M. Kaiser, S. Pereira, L. Pohl, S. Ketelhut, B. Kemper, C. Gorzelanny, H.-J. Galla, B.M. Moerschbacher, F.M. Goycoolea, Chitosan encapsulation modulates the effect of capsaicin on the tight junctions of MDCK cells., Sci. Rep. 5 (2015) 10048. doi:10.1038/srep10048.

[46] C. Vila-Sanjurjo, C. Remuñán-López, L. David, C. Rochas, F.M. Goycoolea, Interference with a bacterial quorum sensing-based response by sub-lethal levels of chitosan

nanoparticles. Submitted, (n.d.).

[47] B. Santos-Carballal, L.J. Aaldering, M. Ritzefeld, S. Pereira, N. Sewald, B.M. Moerschbacher, M. Götte, F.M. Goycoolea, Physicochemical and biological characterization of chitosan-microRNA nanocomplexes for gene delivery to MCF-7 breast cancer cells., Sci. Rep. 5 (2015) 13567. doi:10.1038/srep13567.

[48] P. Calvo, J. Alonso, Evaluation of cationic polymer-coated nanocapsules as ocular drug carriers, Int. J. Pharm. 153 (1997) 41–50.

[49] Celina Vila-Sanjurjo, C. Engwer, X. Qin, C. Remuñán-López, A. Vila-Sanjurjo, F.M. Goycoolea, Percolation theory can explain primordial forms of cell-to-cell communication. submitted, (n.d.).

[50] M. Elimelech, J. Gregory, X. Jia, R.A. Williams, Particle Deposition and Aggregation - Measurement, Modelling and Simulation, Elsevier, 1995.

[51] [51] V. Filipe, A. Hawe, W. Jiskoot. Critical evaluation of nanoparticle tracking analysis (NTA) by nanosight for the measurement of nanoparticles and protein aggregates. Pharm. Res. 27 (2010)796-810. doi: 10.1007/s11095-010-0073

[52] E. Van Der Pol, A.G. Hoekstra, A. Sturk, C. Otto, T.G. Van Leeuwen, R. Nieuwland, Optical and non-optical methods for detection and characterization of microparticles and exosomes, J. Thromb. Haemost. 8 (2010) 2596–2607. doi:10.1111/j.1538-7836.2010.04074.x.

[53] H.F.T. Roselena S. Schuh, Fernanda Bruxel, Physicochemical Properties of Lecithin-based nanoemulsions obtained by spontaneous emulsification or high-pressure homogenization. Quim. Nov. 37 (2014) 1193–1198.

[54] C.O. Dimkpa, A. Calder, P. Gajjar, S. Merugu, W. Huang, D.W. Britt, J.E. McLean, W.P. Johnson, A.J. Anderson, Interaction of silver nanoparticles with an environmentally beneficial bacterium, Pseudomonas chlororaphis, J. Hazard. Mater. 188 (2011) 428–435. doi:10.1016/j.jhazmat.2011.01.118.

[55] D. Natrajan, S. Srinivasan, K. Sundar, A. Ravindran, Formulation of essential oil-loaded chitosan–alginate nanocapsules, J. Food Drug Anal. 23 (2015) 560–568. doi:10.1016/j.jfda.2015.01.001.

[56] A. Sarkar, B. Murray, M. Holmes, R. Ettelaie, A. Abdalla, X. Yang, In vitro digestion of Pickering emulsions stabilized by soft whey protein microgel particles: influence of thermal treatment, Soft Matter. 12 (2016) 3558–3569. doi:10.1039/C5SM02998H.

[57] E.I. Rabea, M.E.T. Badawy, C. V. Stevens, G. Smagghe, W. Steurbaut, Chitosan as antimicrobial agent: Applications and mode of action, Biomacromolecules. 4 (2003) 1457–1465. doi:10.1021/bm034130m.

[58] J.S. Kim, E. Kuk, K.N. Yu, J.-H. Kim, S.J. Park, H.J. Lee, S.H. Kim, Y.K. Park, Y.H. Park, C. Hwang, Y. Kim, Y. Lee, D.H. Jeong, M. Cho, Antimicrobial effects of silver nanoparticles, Nanomedicine Nanotechnology, Biol. Med. 3 (2007) 95–101. doi:10.1016/j.nano.2006.12.001.

[59] B. García-Lara, M.Á. Saucedo-Mora, J.A. Roldán-Sánchez, B. Pérez-Eretza, M. Ramasamy, J. Lee, R. Coria-Jimenez, M. Tapia, V. Varela-Guerrero, R. García-Contreras, Inhibition of quorum-sensing-dependent virulence factors and biofilm formation of clinical and environmental Pseudomonas aeruginosa strains by ZnO nanoparticles, Lett. Appl. Microbiol. 61 (2015) 299–305. doi:10.1111/lam.12456.

[60] J.F.P. Wang, Xin, T.R. Romeo, The pgaABCD Locus of Escherichia coli Promotes the Synthesis of a Polysaccharide Adhesin Required for Biofilm Formation, J. Bacteriol. 186 (2004) 2724–2734. doi:10.1128/JB.186.9.2724.

[61] E. Karatan, P. Watnick, Signals, Regulatory Networks, and Materials That Build and Break Bacterial Biofilms, Microbiol. Mol. Biol. Rev. 73 (2009) 310–347. doi:10.1128/MMBR.00041-08.

[62] C. Niu, S. Afre, E.S. Gilbert, Subinhibitory concentrations of cinnamaldehyde interfere with quorum sensing, Lett. Appl. Microbiol. 43 (2006) 489–494. doi:10.1111/j.1472-765X.2006.02001.x.

[63] G. Brackman, T. Defoirdt, C. Miyamoto, P. Bossier, S. Van Calenbergh, H. Nelis, T. Coenye, Cinnamaldehyde and cinnamaldehyde derivatives reduce virulence in Vibrio spp. by decreasing the DNA-binding activity of the quorum sensing response regulator LuxR., BMC Microbiol. 8 (2008) 149. doi:10.1186/1471-2180-8-149.

Table 1. Physical characteristics of nanocapsules and nanoemulsions as determined by dynamic light scattering (DLS-NIBS), nanotroacking analysis (NTA), and phase analysis light scattering and mixed laser Doppler velocimetry (M3-PALS) at 25 °C. Unless otherwise stated, values represent mean average ± S.D. (n = 3).

System	DLS-NIBS		M3-PALS	NTA	
	Z-av.[a] (d., nm)	PdI[b]	Zeta potential (mV)	Mean[c] (d., nm)	Conc.[d] x 10^{-12}/mL
Nanocapsules	155±55	0.127	+50±4	114±31	5.95±0.35
Nanoemulsions	128±41	0.103	-39±2	141±39	10.3±0.14

[a]Z-average diameter ± PdI width; [b] Absolute PdI; [c] Mean size ± standard deviation;
[d] Concentration in number of particles per milliliter of the undiluted stocks of nanocapsules and nanoemulsions.

Table 2. List of parameters and their values used in in silico simulation

	Parameter	Value	Reference
Nanocapsules	Radius	150 nm	Measured by DLS-NIBS
	Density	0.95 $g \cdot cm^{-3}$	Density of Miglyol 812
	Mass	1.68×10^{-18} kg	Calculated from density
	Zeta potential	+50 mV	Measured by M3-PALS
Bacteria	Length	2 µm	Measured by SEM
	Radius	0.4 µm	Measured by SEM
	Zeta potential	-50 mV	Measured by M3-PALS
	Mass	10^{-15} kg	-
System	Box length	3 µm	-
	Temperature	298 K	Room temperature
	Viscosity	2 mPa·s	Viscosity of M9 medium
	Δt	1 ns	-

Figures Captions

Figure 1. SEM images of (a) nanocapsules (NC) and (b) nanoemulsions (NE), supported on smooth and sterile glass. Under there imaging conditions NC and NE appear as bright spherical

objects < 200 nm in size. Size distribution from nanotracking analysis (NTA) and dynamic light scattering (DLS) measurements (as indicated in legend) of NC (c) and NE (d). Values represent mean average ± S.D. (n = 3).

Figure 2. (a) Variation of the ζ–potential of E. coli Top 10 bacteria (OD_{600} = 0.2) in the presence of varying number of nanocapsules (NC) or nanoemulsions (NE). The blue line shows the ζ–potential of pristine bacteria; (b) Experimental and simulation data (as indicated in legend) of the variation of the fraction (%) of bound NC or NE upon incubation of E. coli Top 10 bacteria (OD_{600} = 0.2) with varying ratio of NC per bacterium; (c) Experimental and simulation data (as indicated in legend) of the variation of the absolute number of bound NC or NE upon incubation of E. coli Top 10 bacteria (OD_{600} = 0.2) with varying number of NC per bacterium. Incubation of bacteria and NC or NE was performed at 4 ˚C during 1 h. All experiments were performed in triplicate (values represent mean average ± S.D., n = 3).

Figure 3. SEM images of (a) Pristine E. coli Top 10 bacteria, and after incubation (4 ˚C during 1 h) with nanocapsules (NC) at varying ratios of NC/bacterium: (b) 36 NC/bacteria; (c and d) 109 NC/bacteria; (e) 362 NC/bacteria; and (f) 3620 NC/bacteria. For imaging, samples were supported on track-etched polycarbonate membranes. Under there imaging conditions bacteria appear as bright rod objects. Polycarbonate support appears as a gray background, and sharply-defined track-etched pores appear as dark circles of ca. 1.2 µm in diameter.

Figure 4. Evolution of the growth (OD_{600}) and GFP fluorescence intensity of E. coli Top 10 AHL-sensitive bacteria during the incubation (37 ˚C) at varying ratios of nanocapsules/bacterium (N/B, as shown in labels) with: (a) Unloaded (blank) nanocapsules (NC); and (b) $3OC_6HSL$-loaded nanocapsules. (c) Variation of the inhibition rate of fluorescence intensity calculated from

traces in (a) and (b) as the deviation from the control of different ratios of NC/bacterium (values represent mean average ± S.D., n = 3).

Colloids and Surfaces B: Biointerfaces 149 (2017) 358-368

Graphical abstract

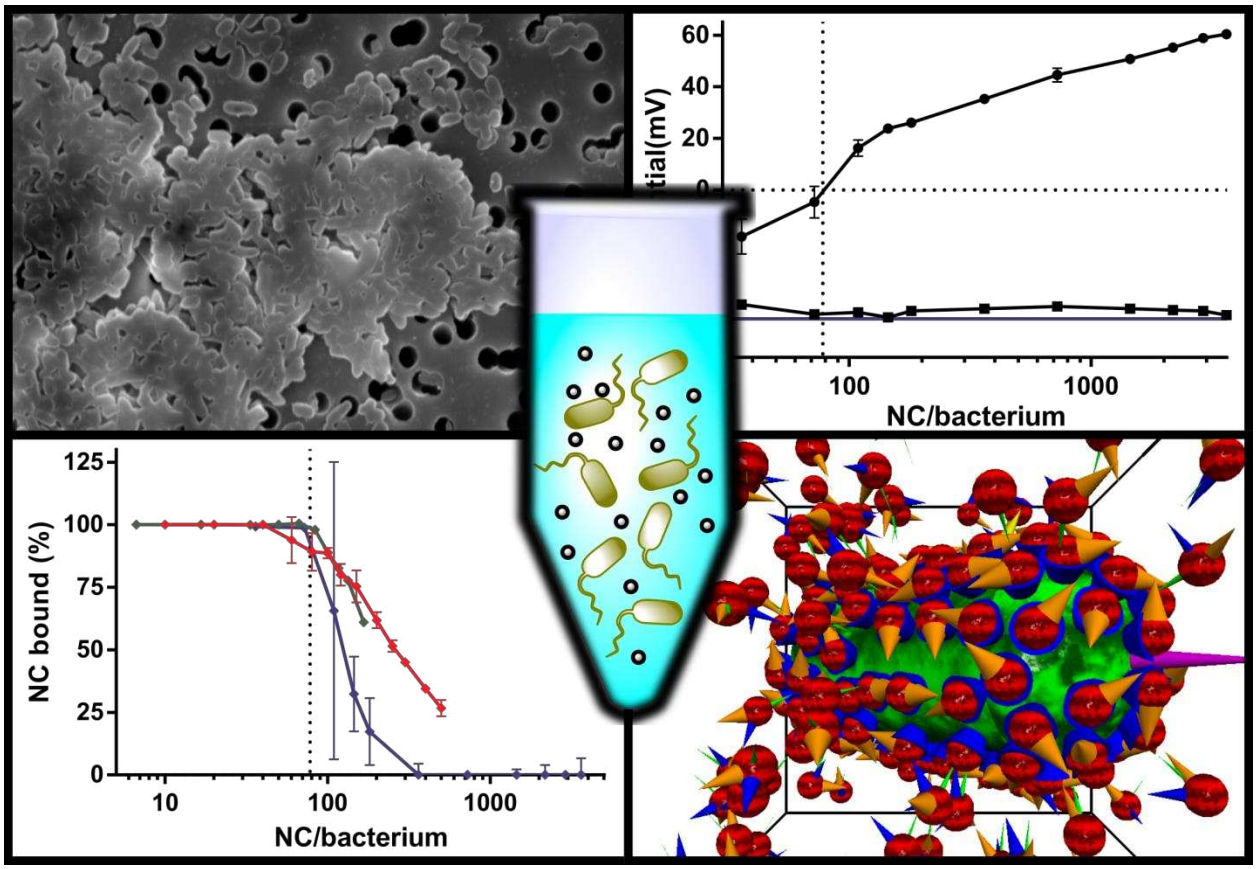

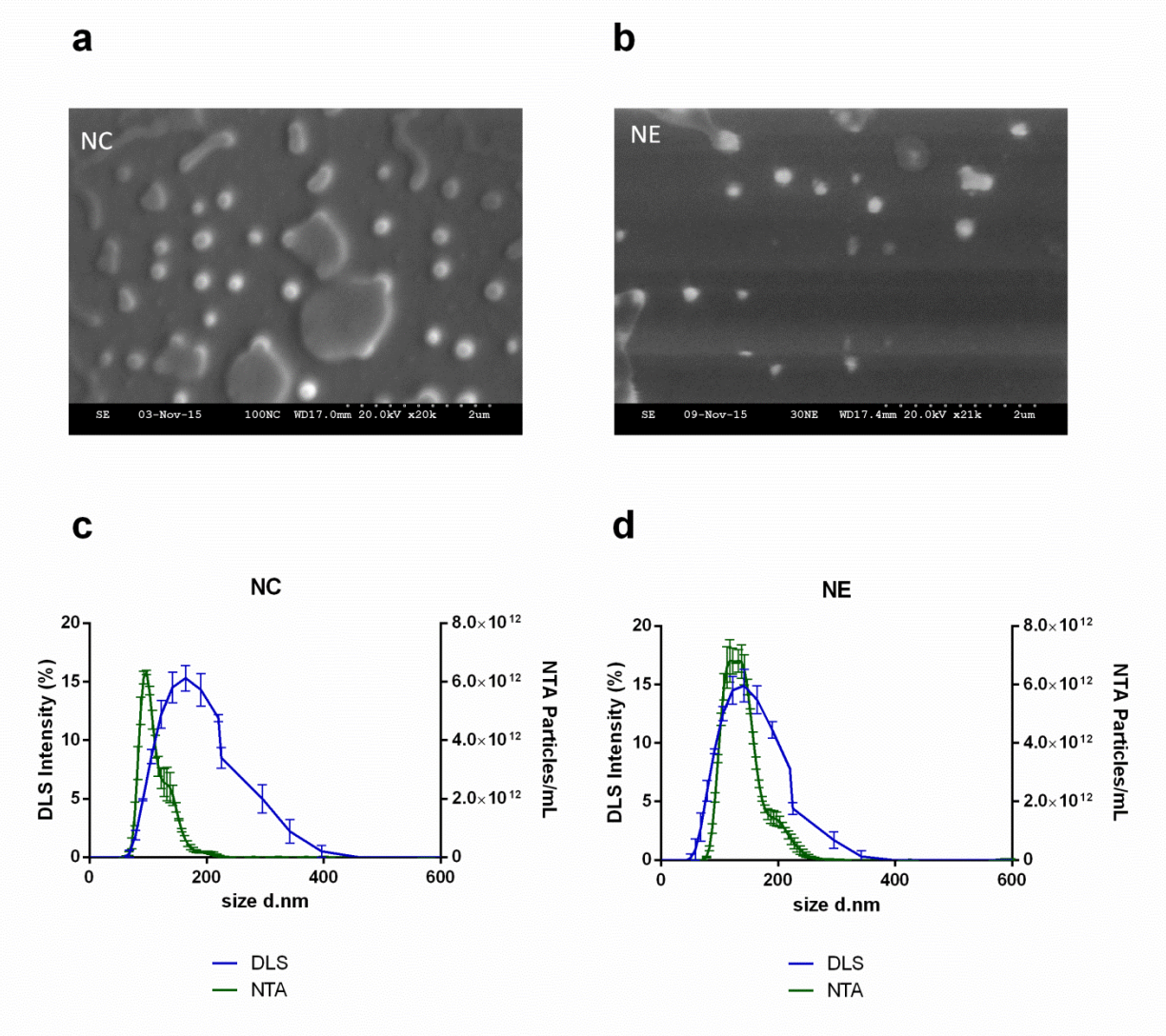
a
b
NC
NE
SE 03-Nov-15 100NC WD17.0mm 20.0kV x20k 2um
SE 09-Nov-15 30NE WD17.4mm 20.0kV x21k 2um
c
d
NC
NE
DLS Intensity (%)
NTA Particles/mL
size d.nm
DLS
NTA

Figure. 1.

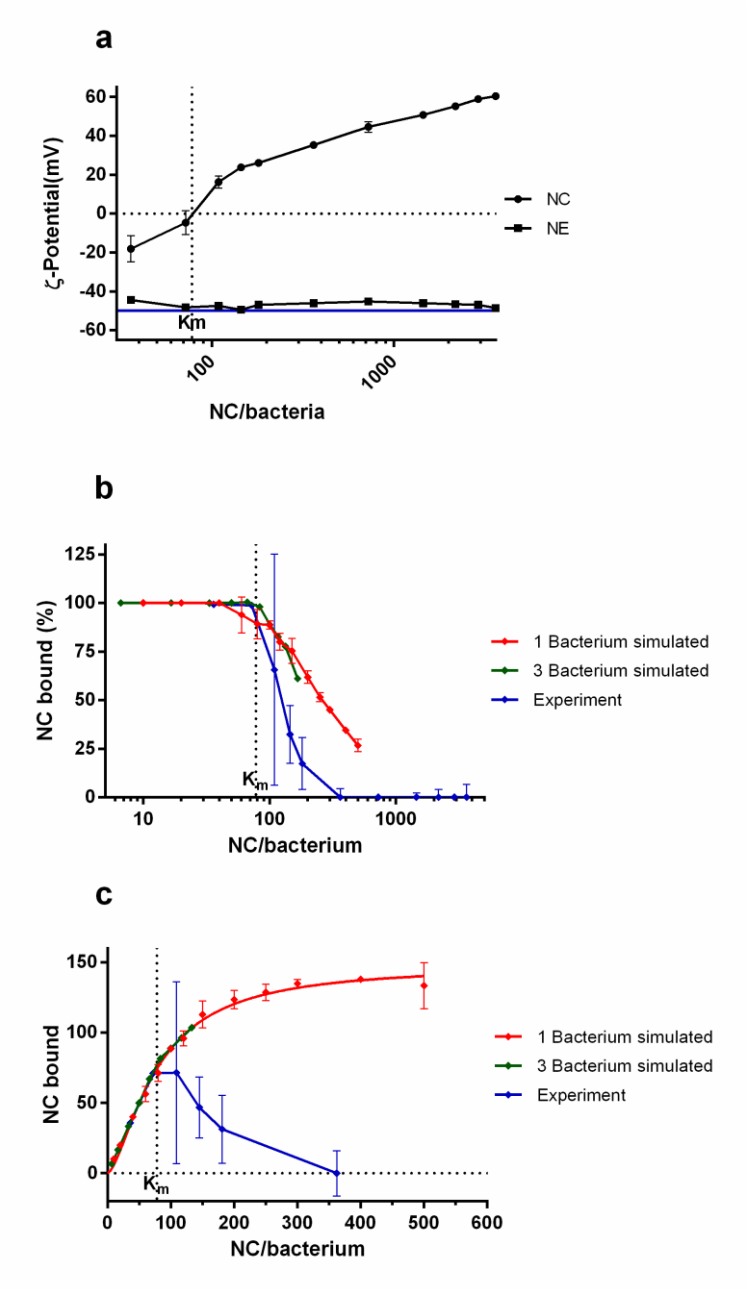
a
ζ-Potential(mV)
60
40
20
0
-20
-40
-60
Km
100
1000
NC/bacteria
NC
NE
b
NC bound (%)
125
100
75
50
25
0
Km
10
100
1000
NC/bacterium
1 Bacterium simulated
3 Bacterium simulated
Experiment
c
NC bound
150
100
50
0
Km
0
100
200
300
400
500
600
NC/bacterium
1 Bacterium simulated
3 Bacterium simulated
Experiment

Fig. 2.

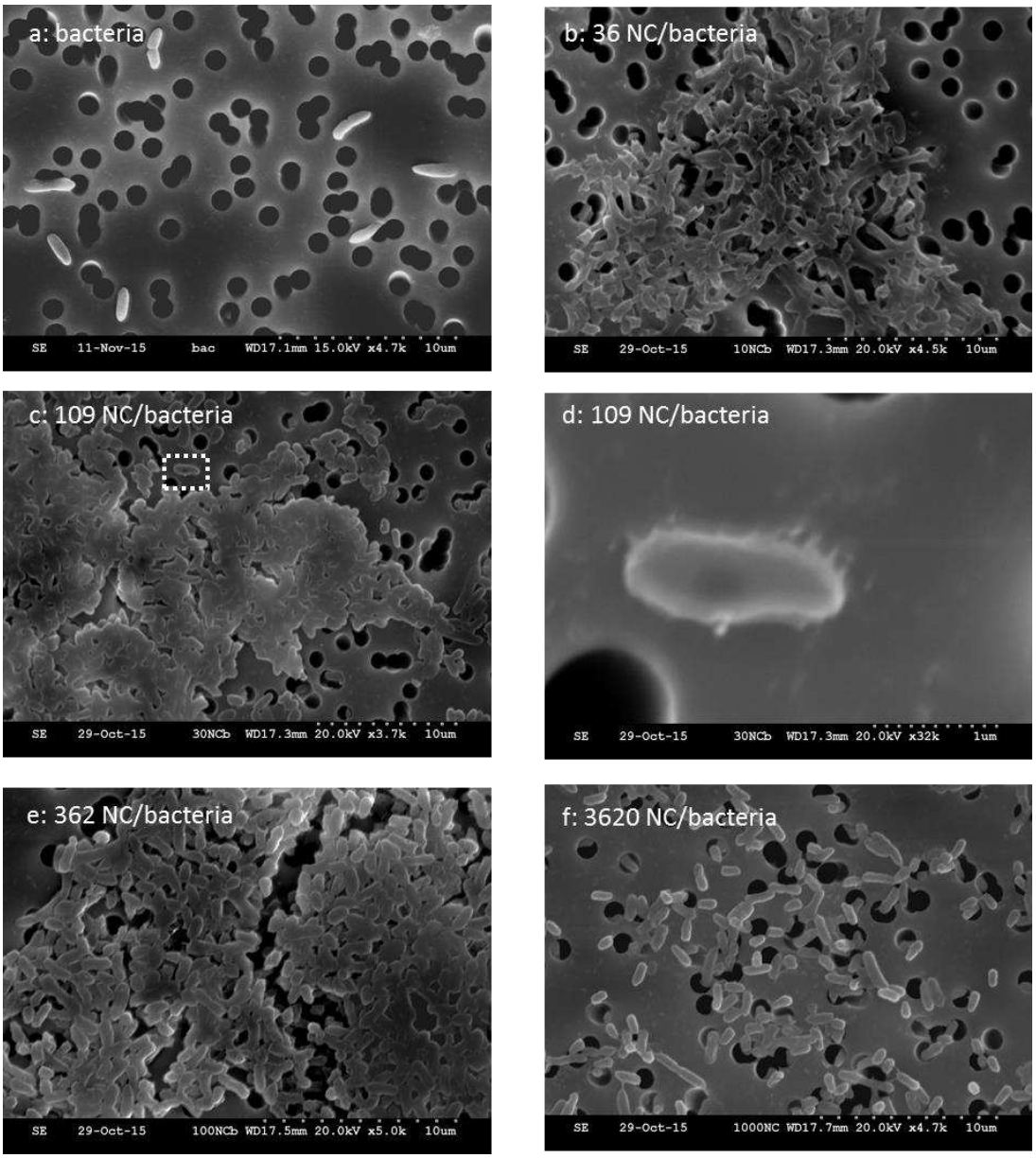
a: bacteria
SE 11-Nov-15 bac WD17.1mm 15.0kV x4.7k 10um
b: 36 NC/bacteria
SE 29-Oct-15 10NCb WD17.3mm 20.0kV x4.5k 10um
c: 109 NC/bacteria
SE 29-Oct-15 30NCb WD17.3mm 20.0kV x3.7k 10um
d: 109 NC/bacteria
SE 29-Oct-15 30NCb WD17.3mm 20.0kV x32k 1um
e: 362 NC/bacteria
SE 29-Oct-15 100NCb WD17.5mm 20.0kV x5.0k 10um
f: 3620 NC/bacteria
SE 29-Oct-15 1000NC WD17.7mm 20.0kV x4.7k 10um

Fig. 3.

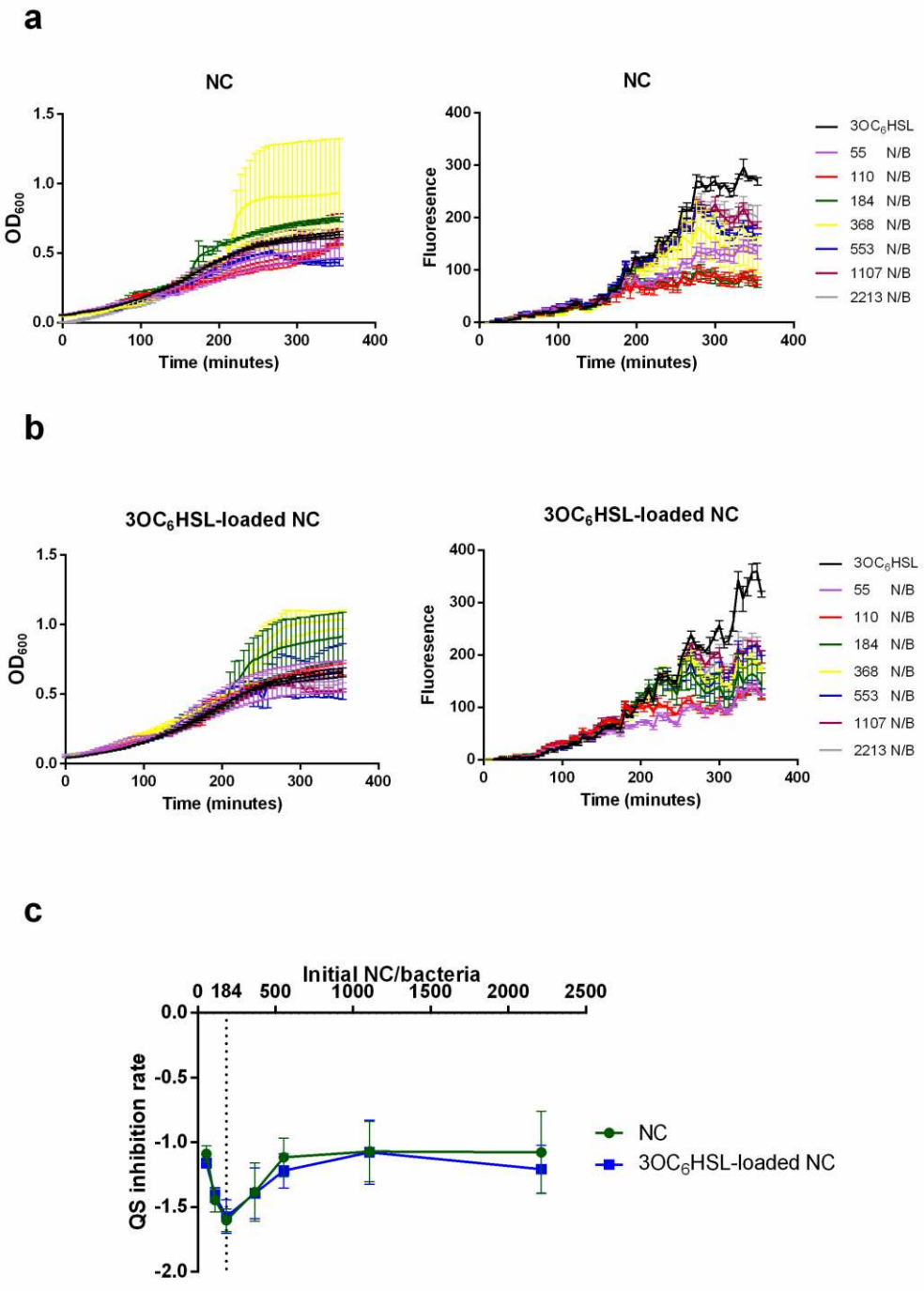
a
NC
NC
OD600
Fluoresence
Time (minutes)
Time (minutes)
3OC6HSL
55 N/B
110 N/B
184 N/B
368 N/B
553 N/B
1107 N/B
2213 N/B
b
3OC6HSL-loaded NC
3OC6HSL-loaded NC
OD600
Fluoresence
Time (minutes)
Time (minutes)
3OC6HSL
55 N/B
110 N/B
184 N/B
368 N/B
553 N/B
1107 N/B
2213 N/B
c
Initial NC/bacteria
0 184 500 1000 1500 2000 2500
QS inhibition rate
NC
3OC6HSL-loaded NC

Fig. 4.

Supplementary Information

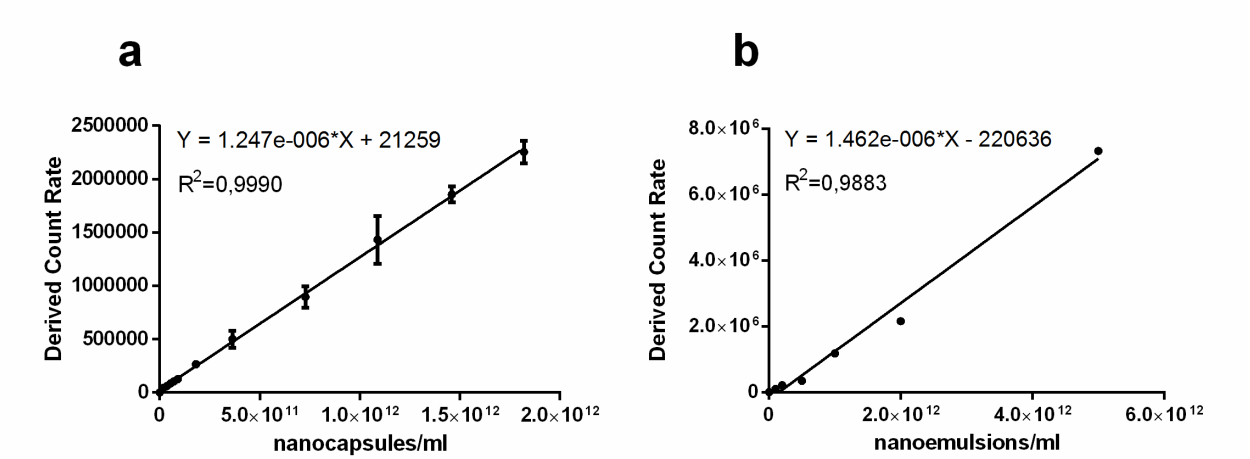

Fig. S1. Calibration curve for the variation of the derived count rate (DCR) with the concentration (number/mL) of: a) nanocapsules; and b) nanoemulsions. The best-fit linear regression data (solid line) and the corresponding equation shown were obtained from GraphPad. values represent mean average ± S.D., n = 3).

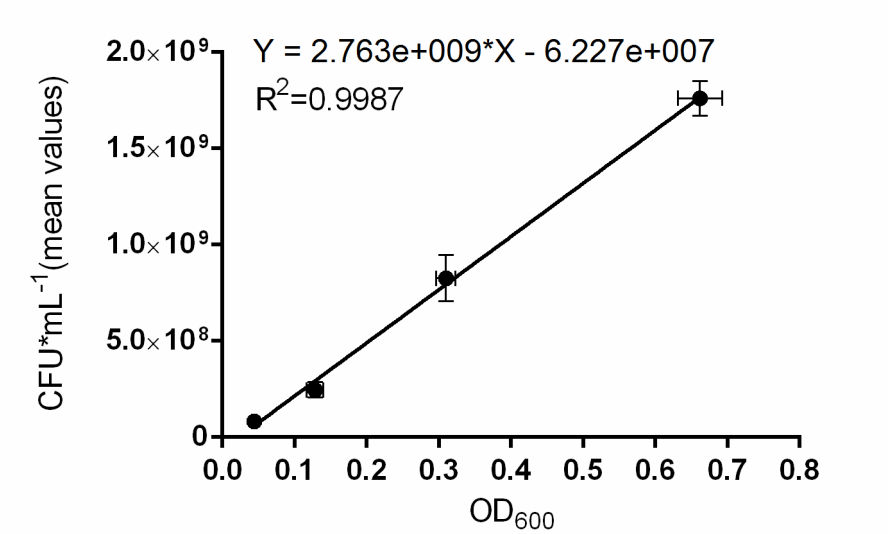

Fig. S2. Calibration curve for the variation of the number of bacteria per unit volume (CFU/mL) with the absorbance (OD_{600}). The best-fit linear regression data (solid line) and the corresponding equation shown were obtained from GraphPad. (values represent mean average ± S.D., n = 3).

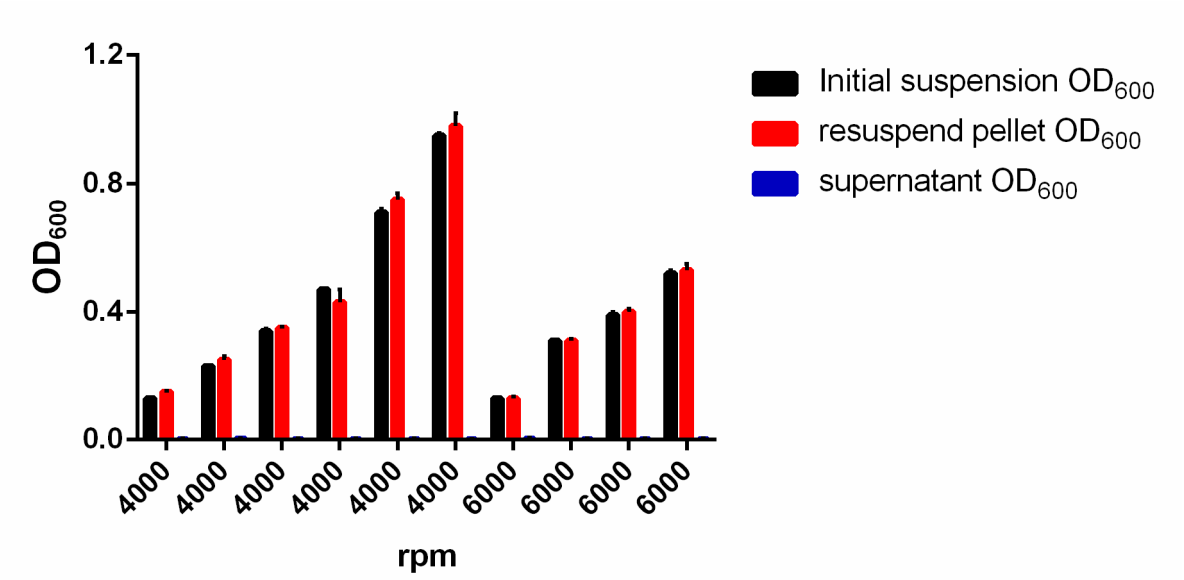

Fig. S3: Variation of the cell density (OD_{600}) of E. coli Top 10 bacteria before and after centrifugation (at 4000 or 6000 rpm during 10 min at 4 ºC) and re-suspending the pellet by vortexing, at varying initial cell densities. The blue bars (almost indiscernible) correspond to the OD_{600} values of the supernatants obtained after centrifugation (values represent mean average ± S.D. , n = 3).

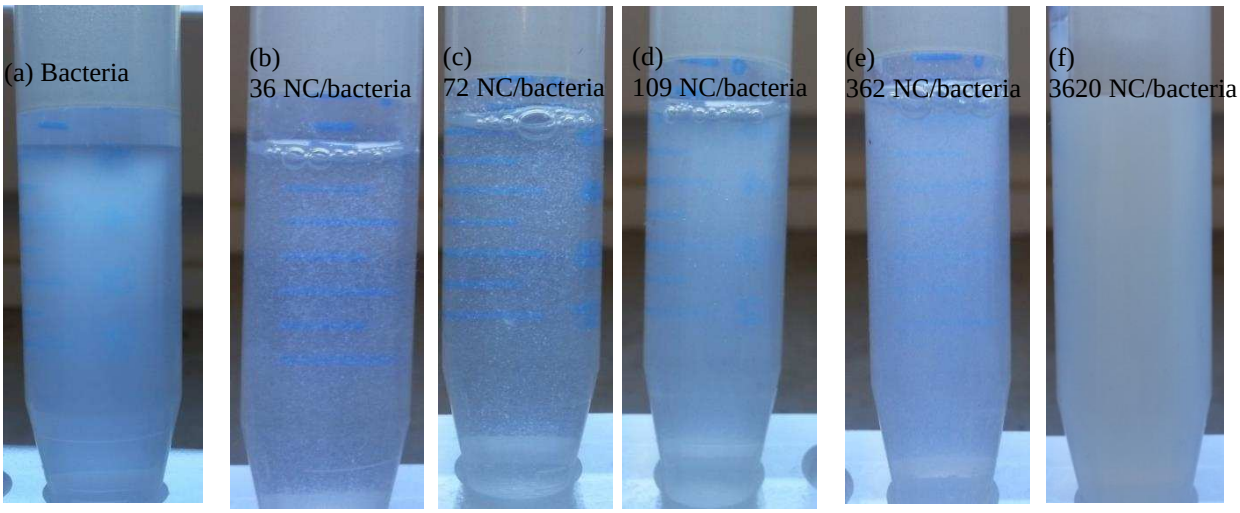

Fig. S4. Visual aspect of representative NC/bacteria suspensions at varying NC/bacterium ratios after incubation at 4 ºC (bacteria suspension OD_{600} = 0.2).

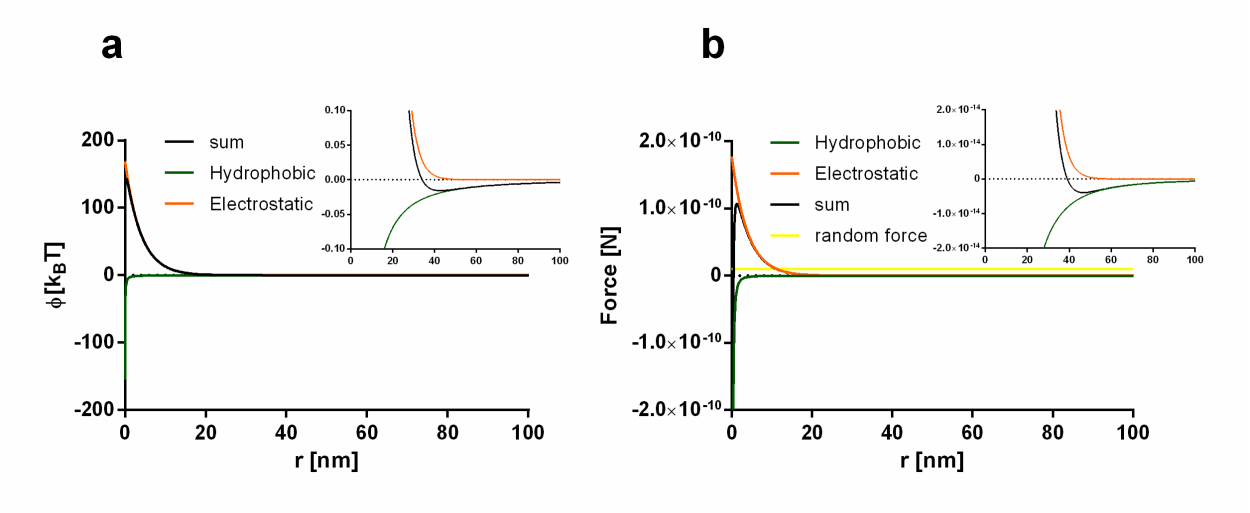

Fig. S5. Interaction potential (a) and interaction forces (b) of two simulated nanocapsules with a diameter of 150 nm and ζ-potential = +50 mV. The overall interaction (defined by the line 'sum') has a Lennard-Jones like nature.

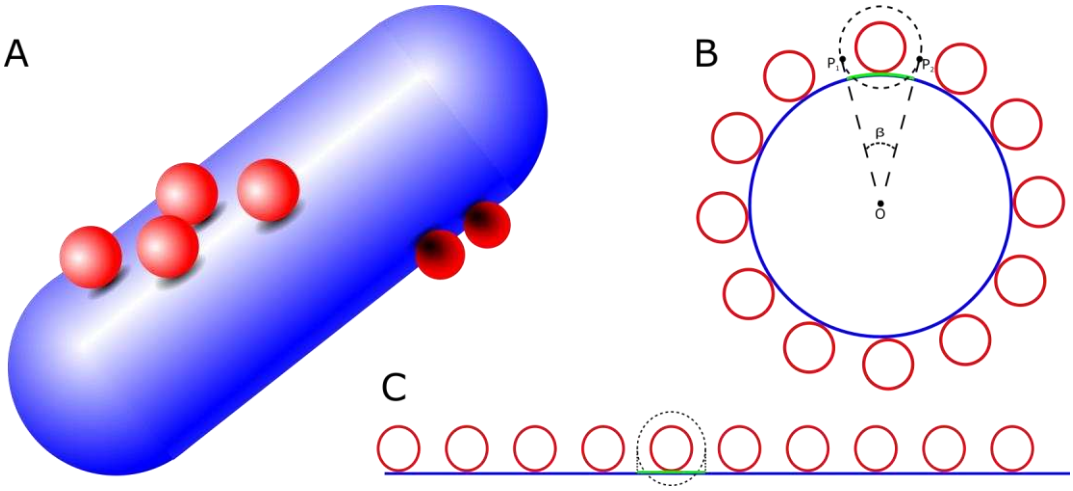

Fig S6. Schematic drawing to illustrate the calculations for the theoretical full coating of a bacterium by nanocapsules.

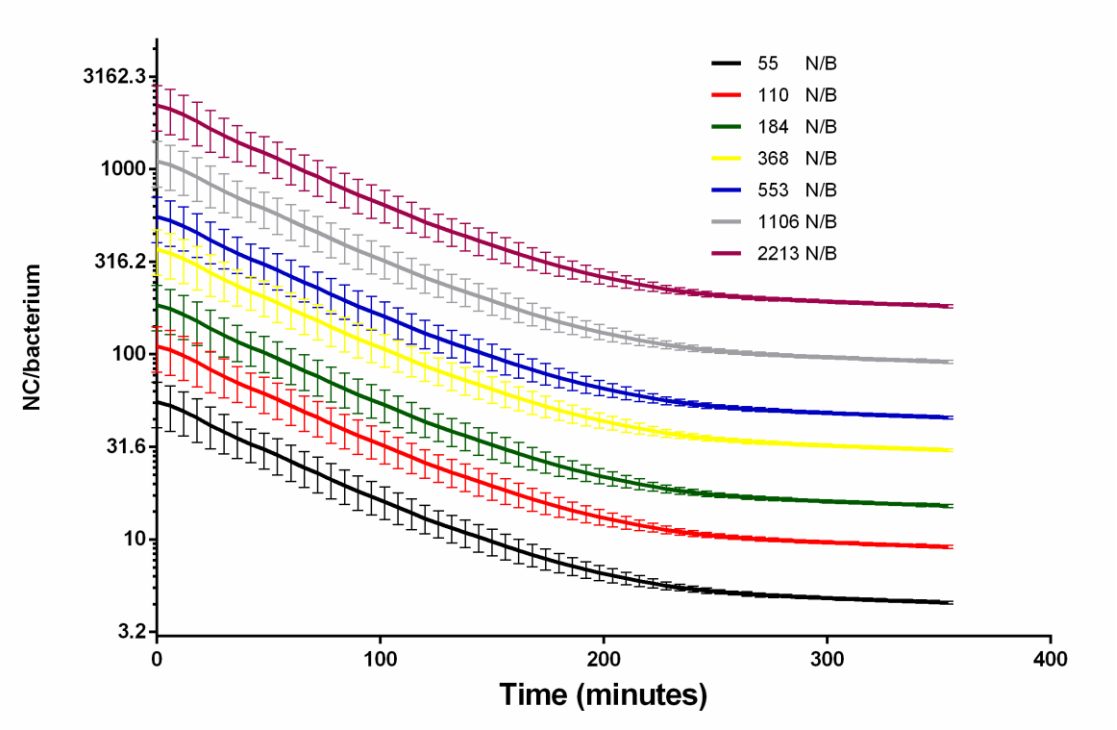

Fig. S7. The ratio of NC/bacteria changing during the time course of a biosensor assay (values represent mean average ± S.D. , n = 3)..

Schematic illustration of the Method to determine number of NC interact with E.coli Top 10 strain

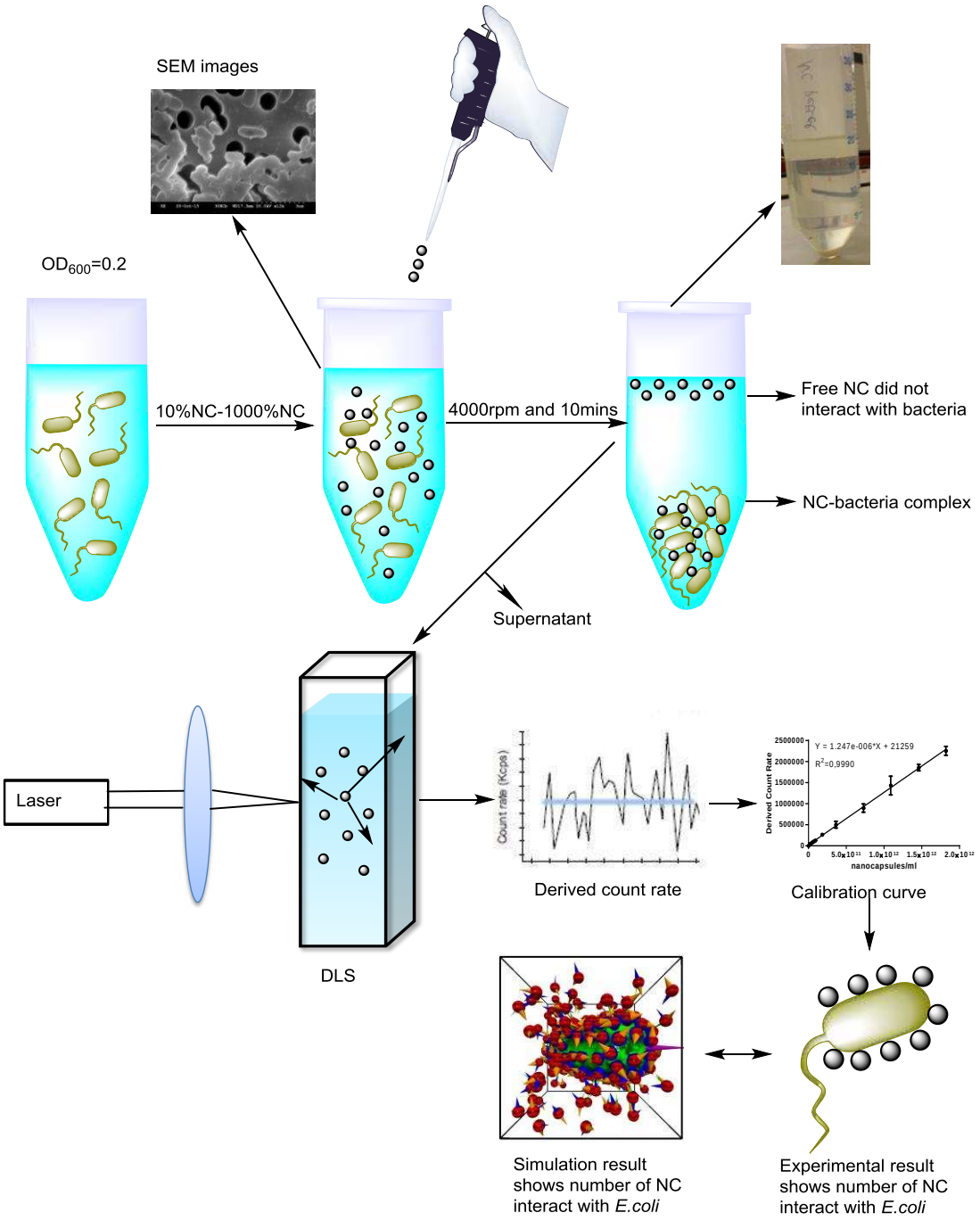

Colloids and Surfaces B: Biointerfaces 149 (2017) 358-368